J. Fluid Mech. (2024), *vol*. 985, A36, doi:10.1017/jfm.2024.279

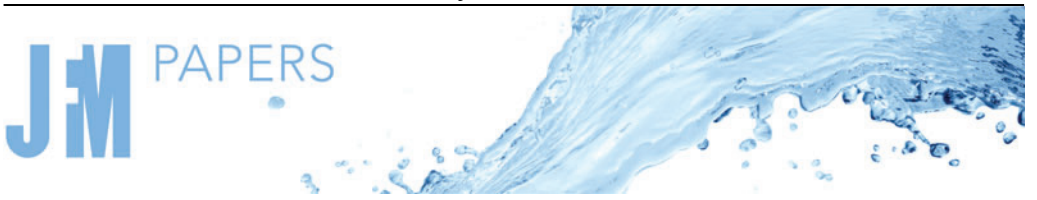

Air-blast atomization of a liquid film

Ippei Oshima[1],† **and Akira Sou**[2]

[1]Institute of Fluid Science, Tohoku University, 2-1-1 Katahira, Aoba-ku, Sendai 980-8577, Japan

[2]Graduate School of Maritime Sciences, Kobe University, 5-1-1 Fukaeminami-machi, Higashinada-ku, Kobe, Hyogo 658-0022, Japan

(Received 26 August 2023; revised 11 March 2024; accepted 11 March 2024)

Air-blast atomizers are extensively used for a variety of purposes. Due to its complexity, the atomization mechanism has not been elucidated. In this study, a mechanistic model is proposed to predict the droplet diameter distribution based on the atomization process of a planar liquid film with co-current gas flows, and its validity is examined by comparing the estimated and measured droplet diameters using high-speed image analysis and laser measurement. As a result, using high-speed imaging, we clarified that the bag film rupture is caused not by the turbulence of the gas flow but by the impact of floating droplets on the liquid film of the expanding bag when the film is thin enough. The average thickness of the liquid film at the bag breakup is of the order of micrometres and varies greatly, resulting in a dispersed distribution of droplet diameters. After the film ruptures, the bag film shrinks towards its transversal and vertical rims due to surface tension, forming large-diameter ligaments. During the contraction process of the bag film, tiny droplets of the order of micrometers are formed at the edge of the perforation. Finally, the remaining ligaments with large diameters fragment into large droplets with submillimetre diameters. The good agreement between the measured and predicted droplet diameter distributions validated the mechanistic model.

Key words: multiphase flow, gas/liquid flows, thin films

1. Introduction

Liquid film air-blast atomization with co-current high-speed gas flows is widely used to produce tiny droplets in numerous applications, including gas turbines, spray painting and spray coating. Figure 1 shows front and side views of a planar liquid sheet with co-current gas flows at a relatively low gas velocity of 40 m s^{-1}, which is smaller than the typical gas

† Email address for correspondence: i.oshima@tohoku.ac.jp

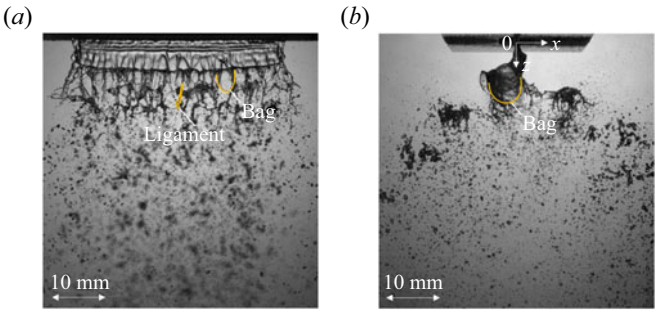

Figure 1. Liquid sheet atomization process with co-current gas flows. (*a*) Front view and (*b*) side view.

velocity in gas turbines. The liquid film oscillates longitudinally due to Kelvin–Helmholtz (KH) instability, transversally due to Rayleigh–Taylor (RT) instability and finally breaks up into droplets. The atomization process is multi-phase and multi-time scale phenomena with various length scales, such as film thickness, atomizer lip thickness, which is the solid wall between the gas and liquid inlet exits, wavelengths of the KH/RT instabilities, bag breakup length, thickness of the boundary layer, turbulence scale and droplet diameter. Due to its complexity, the basic principle of liquid film atomization has not yet been clarified.

Numerous studies on the flapping and breakup processes of liquid films have been conducted owing to the importance of spray diameter prediction and control for many industrial devices. Squire (1953) visualized a sinusoidal fluctuating liquid sheet in stagnant gas and proposed a model for the longitudinal wavelength λ_{Lon} of the liquid sheet. Hagerty & Shea (1955) performed a theoretical analysis of sinusoidal and dilational waves of a liquid film. Fraser *et al.* (1962) and Dombrowski & Hooper (1962) proposed models for the droplet diameter based on theoretical analysis, where a liquid film in this model disintegrates into ligaments and then into droplets by the Rayleigh instability (Rayleigh 1878). The liquid film flapping process with co-current gas flow and with no lip was investigated, and the vortex flow was observed around the film by the numerical simulation (Odier *et al.* 2015). Two different conceptual numerical codes were used to simulate the liquid flapping behaviour, and the usefulness of the Eulerian multi-fluid solver was discussed (Zuzio *et al.* 2013). Lohsea and Villermaux reviewed the rupture of the liquid film based on various influences, such as a laser pulse and heterogeneity of the surface tension (Lohsea & Villermaux 2020). Tang *et al.* simulated the bag breakup of a droplet using the algorithm, in which the liquid film was artificially punctured when it reached a preliminary defined thickness (Tang, Adcock & Mostert 2023). The fragmentation phenomena of films and ligaments are summarized by Villermaux (2006), and the droplet diameter distribution formed by the ligament breakup was discussed by Villermaux *et al.* (2004). They also showed that the droplet diameter distribution produced by the breakup of the liquid film created by the swirl and fan spray nozzles can be expressed as a compound gamma distribution with two parameters (Kooij *et al.* 2018).

Various empirical correlations for the droplet diameter of air-blast atomizers have been proposed by many researchers and summarized by Lefebvre (1980, 1992). However, the previous empirical correlations are mostly available only under limited conditions because these correlations do not take into account all of the complicated atomization processes mentioned above. Therefore, these correlations require parameter tuning for each application and condition.

To develop a mechanistic model for predicting the droplet diameter distribution under a wide variety of conditions, it is necessary to clarify and model all fundamental processes. The flapping phenomena of an air-blasted liquid sheet have been extensively investigated by many researchers. Dumouchel (2008) reviewed atomization characteristics such as the oscillation frequency and breakup length. Using a laser technique, Lozano *et al.* (2005) measured flapping characteristics and proposed an empirical correlation for λ_{Lon}. Considering the effect of lip thickness on the length scale of the gas-phase boundary layer, Oshima *et al.* (2017), Oshima & Sou (2019) proposed a correlation for λ_{Lon} based on the lip momentum ratio MR_{Lip} as a new dimensionless number using D_L because the momentum of the thin liquid film is exchanged downstream of the lip with that of the gas flow. Then, they validated the correlation using their experimental results. Fernandez, Berthoumie & Lavergne (2009) investigated the transversal oscillation phenomenon of a planar liquid film flow and proposed correlations for the transversal wavelength λ_{Tra}. Oshima & Sou (2021) modelled the spanwise oscillation phenomenon based on the RT instability caused by the acceleration of the liquid sheet. Matsuura *et al.* and Yoshida *et al*. studied the effect of the discharged gas flow angle on the droplet diameter using annular and planar liquid sheet atomizers (Matsuura *et al.* 2008; Yoshida *et al.* 2012). Inoue *et al.* investigated the spatial spray flux to determine the local mass ratio of fuel to air in the combustor (Inoue *et al.* 2021). After the longitudinal and transversal oscillations, the liquid film is stretched by the gas flow to form bags. It is well known that the breakup of bags efficiently produces tiny droplets, while the remaining liquid becomes large droplets. There have been numerous foundational studies on thin liquid films and ligaments. The bag breakup of a droplet in a gas flow produces numerous tiny droplets, and a large liquid ring remains. Chou & Faeth (1998) measured the amount of the remaining liquid ring using several liquids and reported that approximately 52 % to 59 % of the original droplet volume became the ring. Taylor (1959) and Culick (1960) proposed a correlation between the film thickness and its velocity based on the relationship between the shrinking velocity of the edge of a liquid film and film thickness. McEntee & Mysels (1969) reconfirmed the validity of the Taylor–Culick velocity model using soap films with a thickness slightly greater than 0.1 μm. When a thin liquid film ruptures and contracts, the contracting rim velocity reaches the Taylor–Culick velocity (Agbaglah, Josserand & Zaleski 2013) and RT instability causes the formation of ligaments at the rim. The breakup of a ligament is based on the Rayleigh instability (Rayleigh 1878) and Weber's theory (Weber 1931; Dombrowski & Johns 1963), which are often used to predict droplet size (Fraser *et al.* 1962; Dombrowski & Johns 1963; Inamura *et al.* 2012). Finally, the remaining liquid that accumulates at the bag rim breaks up into large droplets.

In the recent work, the bag formation process of a liquid film flow on the wall by the gas flow was observed and the effect of the viscosity on the bag length was examined (Kant *et al.* 2023). Jackiw and Asgriz examined the model for predicting droplet diameters in the bag breakup process of a droplet. Based on their visualization and theoretical analysis, they discussed each part of the rim and node. However, the tiny droplets caused by the liquid film rupture were not discussed in detail (Jackiw & Ashgriz 2022). The numerical simulation of the pre-filming air-blast atomizer was compared with their experimental results such as breakup length and droplet diameters (Warncke *et al.* 2017). The effect of the nozzle structure on the liquid film deformation from the pre-filming air-blast atomizer was investigated by numerical simulation (An *et al.* 2023). Thus, there is interest in the deformation and breakup processes of the liquid film from various perspectives.

In the present study, we developed a framework for predicting the droplet distribution based on the phenomenological approach described above rather than

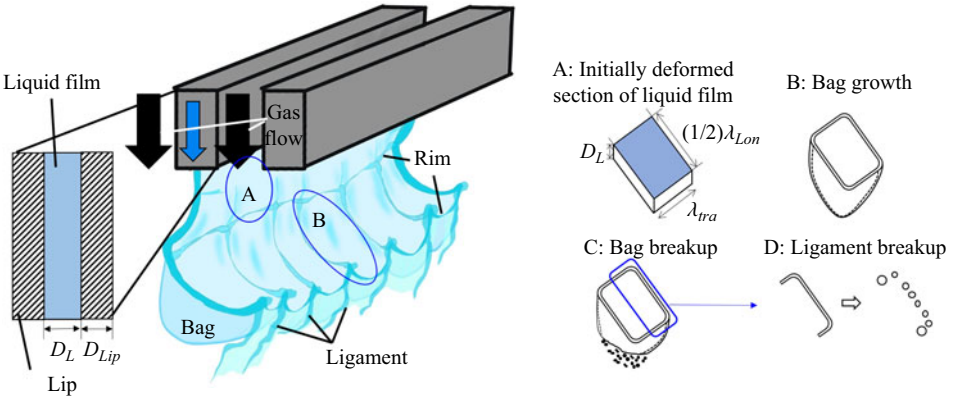

Figure 2. Atomization model of an air-blasted liquid film.

empirical correlation. We first predicted the longitudinal and transversal wavelengths of the oscillating liquid film by the KH–RT instability, which corresponds to the bag sizes. Then, we calculated the diameter of the tiny droplets produced at the contracting film edge after the rupture and the diameter of the large droplet transformed from the remaining liquid. To validate the proposed model, high-speed visualizations of the atomization process of a planar liquid film with co-current gas flows were performed, and the diameters using a Phase Doppler Interferometer (PDI) system and image analysis were measured to confirm the atomization model.

2. Development of a model to predict droplet size distribution

An outline of the proposed atomization model is illustrated in figure 2. The KH instability causes longitudinal oscillation of a liquid film near the exit of an air-blast atomizer, and the oscillating liquid sheet fluctuates in the transverse direction due to RT instability. The rectangular element of the fluctuating liquid sheet is stretched downstream by the impact of the co-current gas flow to form a bag. After the bag breaks up, tiny droplets form at the edge of the perforation, and the remaining liquid becomes ligaments, eventually becoming large drops. In the following sections, we explain the correlations used to predict the diameters of the small and large droplets.

2.1. *Longitudinal wavelength λ_{Lon}*

The liquid film oscillates longitudinally owing to KH instability, and the longitudinal wavelength λ_{Lon} is written as follows (Oshima & Sou 2019):

$$\frac{\lambda_{Lon}}{D_{Lip}} = \frac{14.3}{\sqrt{MR_{Lip}}}, \tag{2.1}$$

where D_{Lip} is the lip thickness. MR_{Lip} is the lip momentum ratio, which is defined as follows:

$$MR_{Lip} = \frac{\rho_G V_G^2 D_{Lip}}{\rho_L V_L^2 D_L}, \tag{2.2}$$

where ρ_G and ρ_L are the densities of the gas and liquid, respectively, V_G and V_L are the gas and liquid velocities, respectively, and D_L is the initial thickness of the liquid sheet.

2.2. *Transversal wavelength λ_{Tra}*

After the longitudinal oscillation of the liquid film by the KH instability, the RT instability induces the spanwise fluctuation of the liquid film, whose acceleration is caused first by the KH instability and then by the drag force of the co-current gas flow. In this study, we tentatively calculate the transversal wavelength λ_{Tra} as (Oshima & Sou 2021)

$$\lambda_{Tra} = c\lambda_{KH}, \tag{2.3}$$

where λ_{KH} is the transversal wavelength based on the acceleration caused by the KH instability, and the coefficient c is given by

$$c = \begin{cases} 0.5, & \text{if } \lambda_{KH} > 2\lambda_{Drag} \\ 1, & \text{otherwise.} \end{cases} \tag{2.4}$$

When $\lambda_{KH} > 2\lambda_{Drag}$, the bag can be deformed into two horizontal bags. Here, λ_{Drag} is the transversal wavelength due to the acceleration caused by the aerodynamic force of the gas flow. These wavelengths are given by

$$\lambda_{KH} = \frac{2\pi}{\omega_{i\_KH}}\sqrt{\frac{3\sigma}{\rho_L D_{Lip}}}, \tag{2.5}$$

$$\lambda_{Drag} = \frac{2\pi}{V_G - V_L}\sqrt{\frac{6\sigma D_L}{\rho_G C_D}}, \tag{2.6}$$

where σ is the surface tension, and C_D is the drag coefficient with a value of 2.0 (Varga, Lasheras & Hopfinger 2003). The growth rate ω_{i_KH} of the horizontal liquid sheet disturbance can be expressed as follows (Squire 1953):

$$\omega_{i\_KH} = \frac{k\sqrt{\dfrac{\rho_G \coth(kD_L)}{\rho_L}}}{1 + \dfrac{\rho_G \coth(kD_L)}{\rho_L}}\sqrt{(V_G - V_L)^2 - \frac{\sigma k}{\rho_G}\left[1 + \frac{\rho_G \coth(kD_L)}{\rho_L}\right]}, \tag{2.7}$$

where k is the wavenumber of λ_{Lon}, which is given by

$$k = \frac{2\pi}{\lambda_{Lon}}. \tag{2.8}$$

2.3. *Volumes of a bag and ligaments*

A bag was formed between the two transverse rims and two vertical rims created by the KH and RT instabilities, as illustrated in figure 2. The distance between the two transverse rims is half that of λ_{Lon}, and that of the vertical rims is λ_{Tra}. Therefore, the volume v of liquid forming the bag is expressed as follows:

$$v = \tfrac{1}{2}\lambda_{Lon}\lambda_{Tra}D_L. \tag{2.9}$$

As soon as the bag is perforated, tiny droplets are formed at the hole edge. Finally, the remaining liquid forms a rim, ligament and droplet. It was reported that 44 % of the droplet

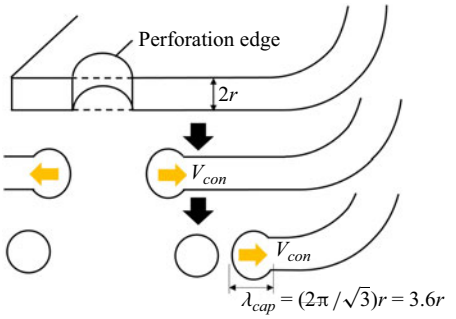

Figure 3. Cross-sectional structure of the moving edge of perforation on a bag.

volume became tiny droplets, and the remaining liquid became a ligament after the bag breakup (Chou & Faeth 1998). Thus

$$v_B = 0.44v, \tag{2.10}$$

$$v_{Li} = 0.56v, \tag{2.11}$$

where v_B and v_{Li} are the total volumes of tiny droplets and ligaments, respectively.

2.4. *Diameters of tiny droplets generated at the hole edge*

A liquid element expands downstream by the co-current gas flow and breaks up. As illustrated in figure 3, the edge of the liquid film with $2r$ thickness moves toward the rim of the bag with V_{con} at a constant velocity after a perforation due to the surface tension force. In other words, the perforation expands, and the liquid film shrinks with V_{con} at the terminal velocity given by Culick (1960) as follows:

$$V_{con} = \sqrt{\frac{\sigma}{\rho_L r}}. \tag{2.12}$$

The equation takes the time t_{trans} for the moving velocity of the perforation edge to reach the Taylor–Culick velocity V_{con}, which is given as follows:

$$t_{trans} \sim O\left(\sqrt{\frac{\rho_L r^3}{\sigma}}\right). \tag{2.13}$$

Due to the surface tension, the perforation edge becomes cylindrical, and the wavelength λ_{cap} of the neck is given by

$$\lambda_{cap} = \frac{2\pi}{\sqrt{3}} r. \tag{2.14}$$

Hence, the acceleration a_{Rim} is roughly given as

$$a_{Rim} = \frac{V_{con}}{t_{trans}}. \tag{2.15}$$

As shown in figure 4, in the spanwise direction of the perforation edge, periodic waves are caused by the RT instability based on these accelerations, whose wavelength λ_{Rim} is

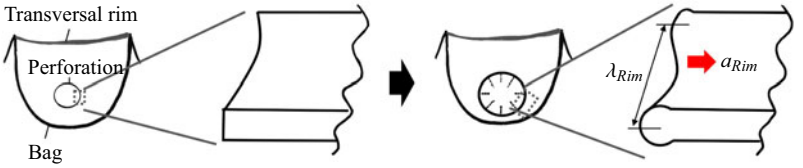

Figure 4. Instability of the moving edge of a perforation.

expressed as

$$\lambda_{Rim} = 2\pi\sqrt{\frac{3\sigma}{\rho_L a_{in}}}, \tag{2.16}$$

where a_{in} denotes acceleration of the perforation edge.

A tiny droplet was formed by the growth of the two horizontal and vertical waves at the perforation edge. The volume of each droplet is calculated as follows:

$$V_{drop\_ba} = 2r\lambda_{Rim}\lambda_{cap} = 8\pi^2 r^2\sqrt{\frac{\sigma}{\rho_L a_{Rim}}}. \tag{2.17}$$

The arithmetic mean diameter D_{Bag} corresponding to V_{drop_ba}, is expressed as follows:

$$D_{Bag} = \left(\frac{6}{\pi}V_{drop\_ba}\right)^{1/3} = \left(\frac{12}{\pi}r\lambda_{Rim}\lambda_{cap}\right)^{1/3} = 2\left(6\pi r^2\sqrt{\frac{\sigma}{\rho_L a_{Rim}}}\right)^{1/3}. \tag{2.18}$$

2.5. *Diameter of large droplets caused by ligament breakup*

Because gas flow does not affect ligament breakup, the Rayleigh or Weber theory (Dombrowski & Johns 1963) is suitable for calculating the droplet diameter. After the bag is ruptured, the remaining liquid, without bag breakup, collects at the transversal and vertical rims and eventually becomes a ligament. The gas flow stretches the bag and the vertical rim between two adjacent bags. The vertical rims are approximately two to four times longer than λ_{Lon}. Therefore, we estimate the length in this study as $3\lambda_{Lon}$. Assuming that the ligament is a uniform cylinder, its radius R is determined from v_{Li} using the following equation satisfying the conservation of the mass as follows:

$$R = \sqrt{\frac{v_{Li}}{\pi(3\lambda_{Lon} + \lambda_{tra})}}. \tag{2.19}$$

The droplet diameter D_{Li} is obtained by the following Weber theory:

$$D_{Li} = 3.76R(1 + 3Oh)^{1/6}, \tag{2.20}$$

where Oh is the Ohnesorge number, which is defined by

$$Oh = \frac{\mu_L}{\sqrt{2\rho_L\sigma R}}. \tag{2.21}$$

2.6. *Summary of a mechanistic model for droplet diameter*

The flowchart of the mechanistic model of the droplet diameter distribution is shown in figure 5. The framework enables us to predict droplet diameters via the above phenomenological modelling on the bag and ligament breakups, which can account for the effects of velocity and physical properties of gas and liquid and injector geometries without any tuning parameters.

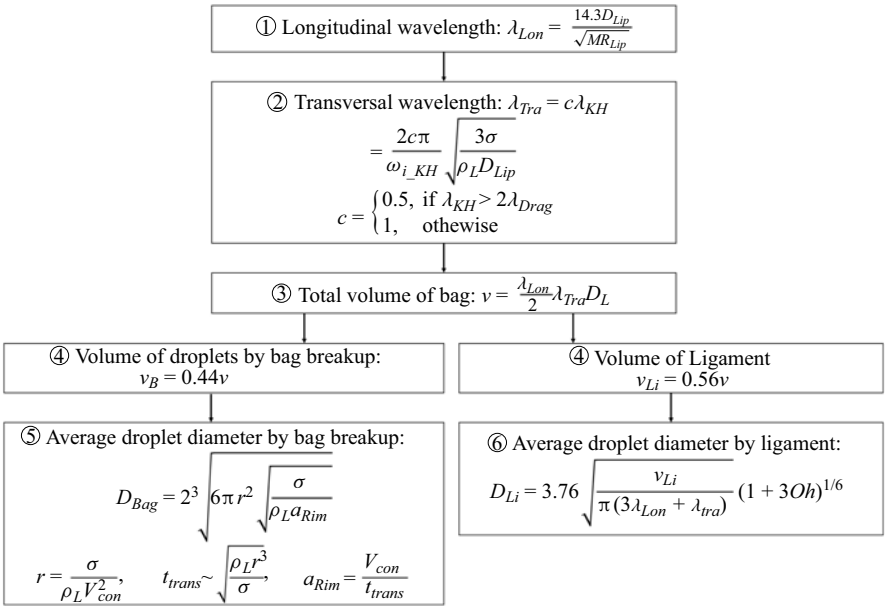

Figure 5. Flow chart of the mechanistic model of the air-blast liquid sheet atomization.

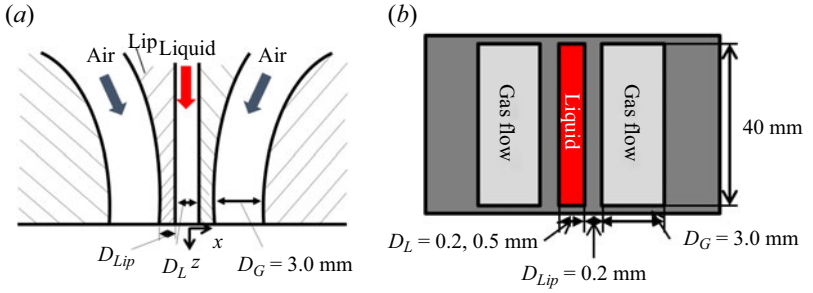

Figure 6. Planar air-blast atomizer for the liquid film.

3. Experimental set-up and conditions

A schematic diagram of the planar air-blast atomizer (Yoshida *et al.* 2012) is shown in figure 6. In the present study, the thickness of a liquid film is 0.2 and 0.5 mm, the width of the gas flow is 3.0 mm and the thickness of the lip is 0.2 mm. We assembled the experimental apparatus shown in figure 7. Pure water at room temperature was injected into the atmosphere using compressed gas. The liquid mass flow was controlled by a needle valve and measured by a Coriolis flow sensor (KEYENCE, FD-SS20A). The blower (HITACHI, VB-030-E3) ejected the gas flow, whose mass flow rate was controlled by rotational control using an inverter, and was measured with a liquid column manometer.

The formation and breakup of bags and ligaments were recorded with a high-speed camera (Vision Research, Phantom v211, and MIRO LAB310). Backlight images were taken with a macro lens (Nikon, AI AF Micro-Nikkor 200 mm f/4D IF-ED), a close-up ring and a metal halide lamp (Kyowa, MID-25FC, SIGMA KOKI, SHLA-150). The acquisition rate was 7000–30 000 f.p.s., and the spatial resolution of the images was chosen to be 20–100 μm pixel^{-1} to sufficiently capture the analysis object.

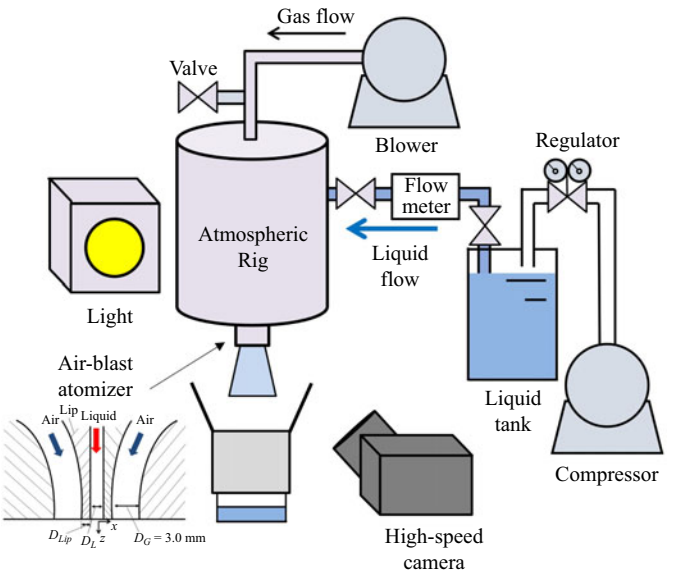

Figure 7. Atmospheric experimental apparatus.

The droplet diameter and velocity were measured using a PDI system (Artium, PDI-200 MD). The collection angle was approximately 70°. The front and back focal lengths were both 500 mm, and the slit aperture was set to 100 μm. The droplets generated by ligament breakup were non-spherical and had a diameter greater than 150 μm. Because almost all droplet diameters measured by the PDI system were less than 100 μm, we eliminated data whose droplet diameters were greater than 100 μm using a filter. We collected 10 000 droplets at each measurement point and examined the burst signals with an oscilloscope. The diameters of the ligaments and droplets generated by ligament breakup were measured using image analysis. Since the diameters of the ligaments were not uniform, we measured the average diameters for each case. After the ligament breakup, the diameters of two hundred large droplets were measured.

4. Results and discussion

4.1. *Visualization of the bag breakup process*

The high-speed images of a typical bag breakup process are shown in figure 8. It was found that bag breakup is almost always triggered, not by turbulence or the Van der Waals force, but by the collision of the rapidly expanding thin liquid film and floating droplets. The ruptured liquid film contracted longitudinally and transversely toward the rims of the bag due to surface tension to retain the ligaments. Many tiny droplets formed at the perforation edge because the liquid film was very thin when the bag ruptured.

When a floating droplet impacts a thick liquid film with comparatively slow expansion velocity prior to the bag's large expansion, the film does not always rupture. The impingement of a droplet on a thick liquid film is shown in figure 9. The preceding observation indicates that the liquid film will only rupture when it is sufficiently thin and the impact velocity is high. We consider the critical Weber number. As we presume that the velocity of the bag expansion is 1 m s^{-1} and liquid film thickness is 10 μm, the critical

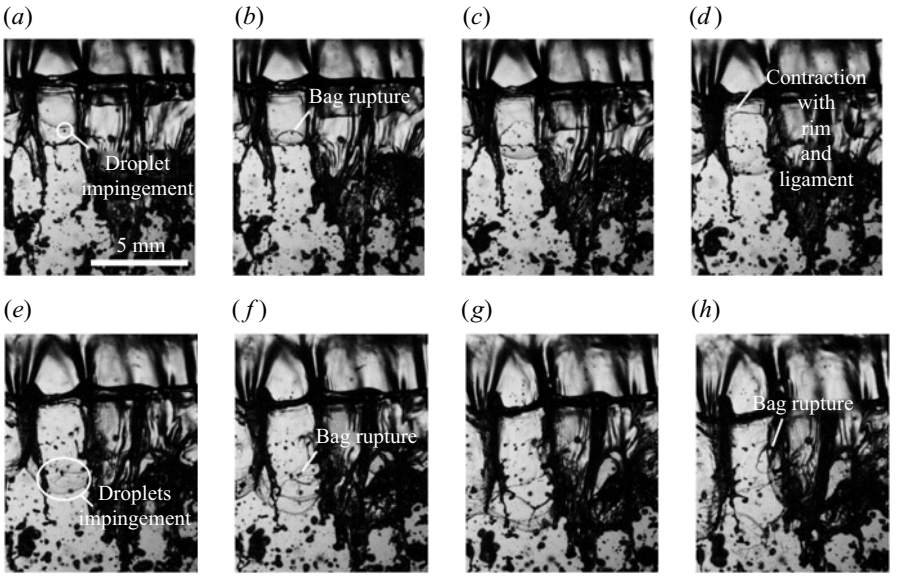

Figure 8. Bag breakup process initiated by a droplet impingement ($D_L = 0.5$ mm, $V_L = 1$ m s^{-1}, $V_G = 30$ m s^{-1}); (*a*) $t = 0$ ms, (*b*) $t = 0.09$ ms, (*c*) $t = 0.18$ ms, (*d*) $t = 0.27$ ms, (*e*) $t = 0.36$ ms, (*f*) $t = 0.45$ ms, (*g*) $t = 0.55$ ms and (*h*) $t = 0.64$ ms.

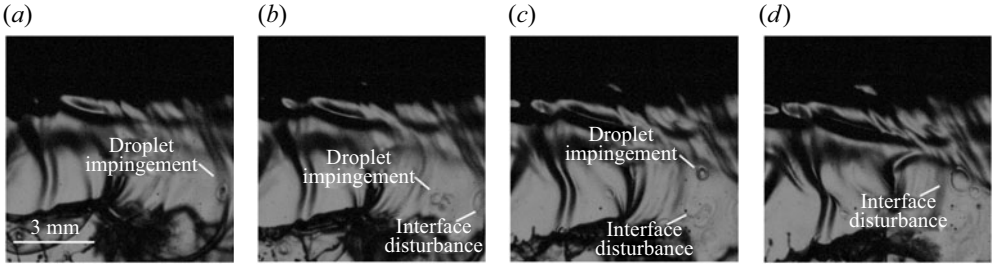

Figure 9. Disturbance wave of a liquid film by the droplet impact ($D_L = 0.2$ mm, $V_L = 1$ m s^{-1}, $V_G = 30$ m s^{-1}); (*a*) 0.12 ms, (*b*) 0.25 ms, (*c*) 0.37 ms and (*d*) 0.49 ms.

Weber number is approximately 0.1. By taking into account the variations in local gas velocity and local film thickness, the critical Weber number is estimated to be about one.

To estimate the diameters of the small droplets we must estimate the film thickness. The measured contracting rim velocities V_{Con} after film rupture are shown in figure 10. Figure 10(*a*) shows an example of the measured V_{Con} distribution, and figure 10(*b*) shows the average V_{Con} in each case. The maximum measurement error in the contraction velocity V_{Con} is estimated to be approximately at most 15 % when we assume that the bag takes the shape of a spheroid and remove the V_{con} data that appear near the bottom of the bags. Therefore, the depth of the field and the viewing angle were controlled in the experiment. The measured V_{Con} values ranged from 3 to 12 m s^{-1}. The effects of V_L and V_G on V_{Con} were insignificant. In this study, we use $V_{Con} = 5$ m s^{-1} at $D_L = 0.5$ mm and $V_{Con} = 7$ m s^{-1} at $D_L = 0.2$ mm as measured data.

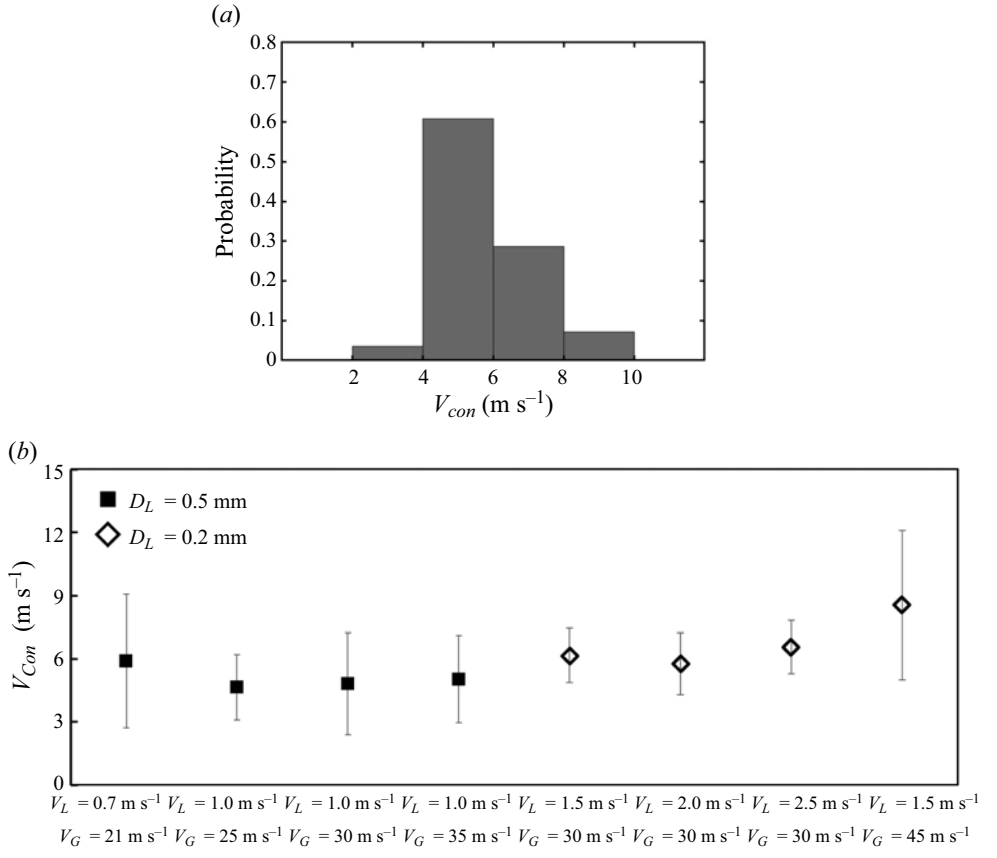

Figure 10. Measured contracting rim velocity V_{Con}. (*a*) Probability at $V_L = 2$ m s^{-1}, $V_G = 30$ m s^{-1} and $D_L = 0.2$ mm and (*b*) average V_{Con}.

4.2. *Visualization of the ligament formation process*

Figure 11 shows the ligament formation process. The upper images show the original, whereas the lower images highlight the perforations edge and longitudinal rims. At $t = 0$ ms, we can see the vertical rims between the bags and the perforation edge. The perforation grows over time. As a result, the vertical rim collects the liquid and transforms into a ligament, and the transverse rim becomes a liquid column with a larger diameter. This process creates tiny droplets when the bag is ruptured, and several ligaments and large liquid columns are formed.

4.3. *Evaluation of the atomization model by the comparison between predicted and measured droplet diameters*

In this section, the estimated droplet diameters obtained with our atomization model are compared with the experimental results to determine the validity of the proposed model. First, the longitudinal and transversal wavelengths λ_{Lon} and λ_{Tra} are predicted using (2.1) and (2.3). The validity of λ_{Lon} and λ_{Tra} correlations have been confirmed (Oshima & Sou 2019, 2021). The bag volume, v, was calculated using λ_{Lon} and λ_{Tra}. Figure 12 shows the estimated v. As V_L and D_L increase, v increases, whereas an increase in V_G decreases v. The discontinuity appears at low V_G due to the switching in the dominant acceleration for

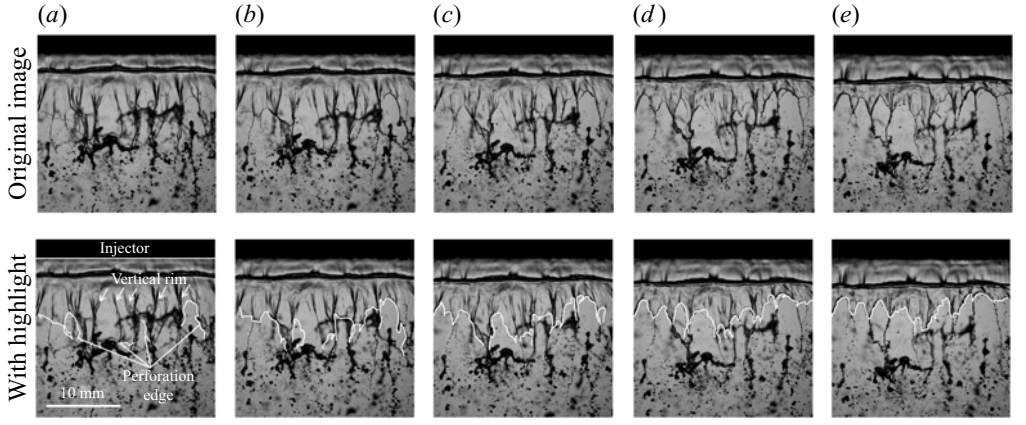

Figure 11. Ligament formation process after the bag breakup ($D_L = 0.2$ mm, $V_L = 1.5$ m s^{-1}, $V_G = 30$ m s^{-1}); (*a*) $t = 0$ ms, (*b*) $t = 0.14$ ms, (*c*) $t = 0.28$ ms, (*d*) $t = 0.41$ ms and (*e*) $t = 0.55$ ms.

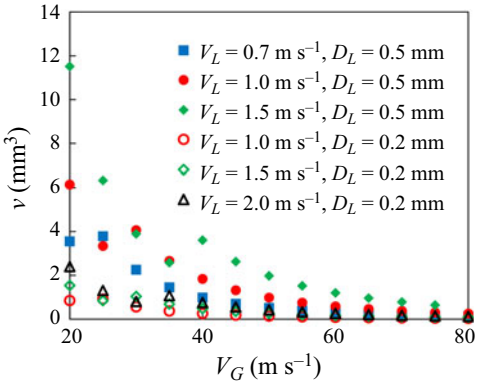

Figure 12. Predicted volume of a bag.

the RT instability, and its effect is involved in the coefficient c of (2.3). It was confirmed that the nonlinear transition of λ_{Tra} occurred from the measurement (Oshima & Sou 2021).

The volume of the ligament v_{Li} was obtained from (2.11), which was used to calculate the radius of the ligament R using (2.20). The predicted and measured R are shown in figure 13. The error bar indicates the standard deviations. As V_G increases or V_L decreases, R also decreases. The R decreases slightly when D_L decreases. The mean error of the predictions at $D_L = 0.5$ mm was 16 %, and that at $D_L = 0.2$ mm was 47 %. The predicted and measured results are in good agreement.

The predicted and measured large droplet diameters D_{Li} obtained by ligament breakup are shown in figure 14. The measured value is the mean diameter D_{10} obtained by image analysis, and the error bars represent the standard deviations. Although a simple comparison between the measured and predicted data is not possible due to the large variations in the measured diameters, the predicted and measured data agree that the droplet diameter decreases with increasing V_G or decreasing V_L and D_L. The droplet diameter derived from the transverse rim was strikingly large at a large V_L or low V_G. The mean diameters D_{10} at large V_L or low V_G were slightly larger than the predicted values. The mean error of the predictions at $D_L = 0.5$ mm was 26 %, and that at $D_L = 0.2$ mm

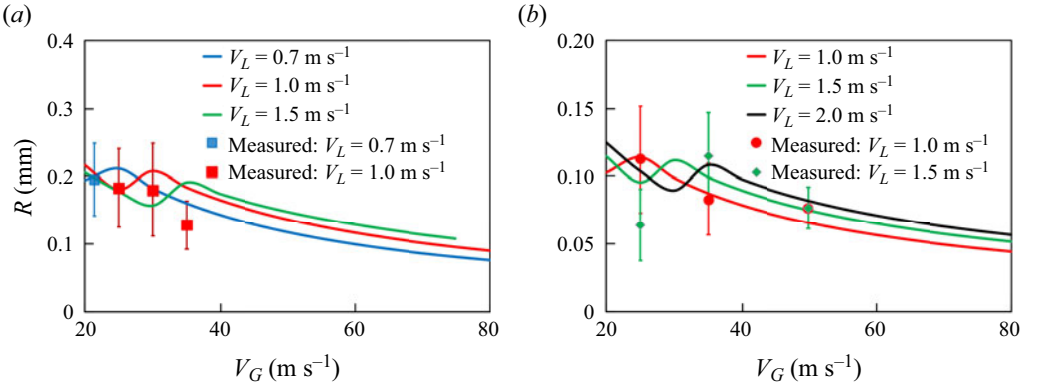

Figure 13. Predicted and measured radius of ligament; (*a*) $D_L = 0.5$ mm and (*b*) $D_L = 0.2$ mm.

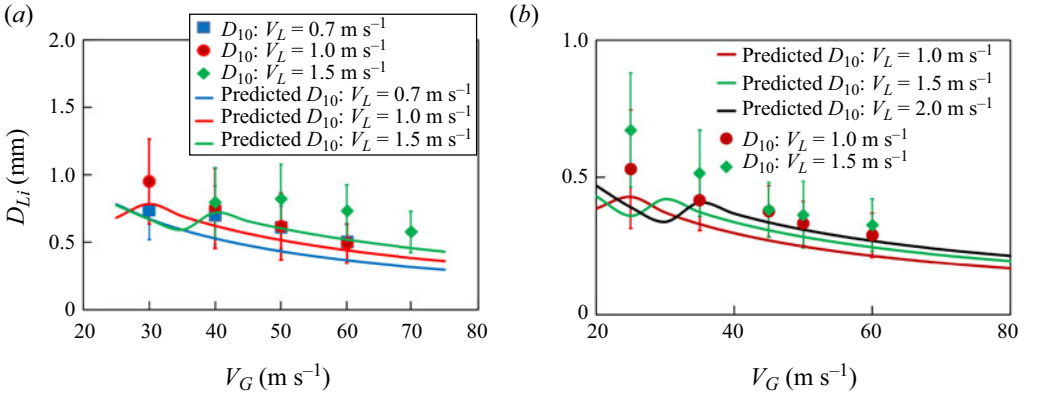

Figure 14. Predicted and measured droplet diameter by ligament breakup; (*a*) $D_L = 0.5$ mm and (*b*) $D_L = 0.2$ mm.

was 31 %. The predicted droplet diameters agreed with the measured values, except in the preceding cases.

Finally, we address the predicted diameters of the small droplets. First, the thickness of the liquid film was estimated. In the present study, we use the average value of the measured V_{Con}, i.e. $V_{Con} = 5$ m s^{-1} at $D_L = 0.5$ mm and $V_{Con} = 7$ m s^{-1} at $D_L = 0.2$ mm. From (2.12), the liquid film thickness $2r$ can be expressed as follows:

$$2r = \begin{cases} \dfrac{2\sigma}{\rho_L V_{con}^2} \sim \dfrac{2 \times 0.072}{998 \times 5^2} \sim 6\,\mu\text{m}, & \text{when } D_L = 0.5 \text{ mm} \\ \dfrac{2\sigma}{\rho_L V_{con}^2} \sim \dfrac{2 \times 0.072}{998 \times 7^2} \sim 3\,\mu\text{m}, & \text{when } D_L = 0.2 \text{ mm}. \end{cases} \tag{4.1}$$

Here, we examined the effect of the varying V_{Con} on $2r$ as a sensitivity analysis. At $V_{Con} = 2$ and 12 m s^{-1}, the minimum and maximum film thicknesses were $2r_{max} \sim 36$ μm and $2r_{min} \sim 1$ μm, respectively. Therefore, $2r$ may have a large deviation, and the non-uniformity of the film thickness may cause a large variation in the droplet size distribution.

Next, we estimated the acceleration at the perforation edge. If the film thickness of bag $2r$ is 6 or 3 μm, the delay time t_{trans} for the edge velocity to reach its terminal velocity

V_{Con}, calculated using (2.13), is as follows:

$$t_{trans} = \begin{cases} 0.58\,\mu\text{s}, & \text{when } D_L = 0.5 \text{ mm} \\ 0.21\,\mu\text{s}, & \text{when } D_L = 0.2 \text{ mm}. \end{cases} \tag{4.2}$$

The acceleration a_{Rim} based on the initial accelerated motion is given as follows:

$$a_{Rim} = \begin{cases} \dfrac{V_{con}}{t_{trans}} \sim \dfrac{5}{5.8 \times 10^{-7}} \sim 8.7 \times 10^6 \text{ m s}^{-2}, & \text{when } D_L = 0.5 \text{ mm} \\ \dfrac{V_{con}}{t_{trans}} \sim \dfrac{7}{2.1 \times 10^{-7}} \sim 3.3 \times 10^7 \text{ m s}^{-2}, & \text{when } D_L = 0.2 \text{ mm}. \end{cases} \tag{4.3}$$

Therefore, the droplet diameter due to bag breakup can be obtained by solving (2.18), using a_{Rim}

$$D_{Bag} = \begin{cases} 2\left[6\pi r^2 \sqrt{\dfrac{\sigma}{\rho_L a_{Rim}}}\right]^{1/3} = 2\left[6\pi (3 \times 10^{-6})^2 \sqrt{\dfrac{0.072}{998 \times 8.7 \times 10^6}}\right]^{1/3} \sim 15\ \mu\text{m}, \\ \qquad\qquad \text{when } D_L = 0.5 \text{ mm} \\ 2\left[6\pi r^2 \sqrt{\dfrac{\sigma}{\rho_L a_{Rim}}}\right]^{1/3} = 2\left[6\pi (1.5 \times 10^{-6})^2 \sqrt{\dfrac{0.072}{998 \times 3.3 \times 10^7}}\right]^{1/3} \sim 8\ \mu\text{m}, \\ \qquad\qquad \text{when } D_L = 0.2 \text{ mm}. \end{cases} \tag{4.4}$$

The D_{Bag} was between 3 μm and 96 μm, since V_{Con} was 2–12 m s^{-1}. It is important to consider the non-uniformity of the bag film thickness when predicting the droplet diameter distribution. The mean droplet diameter decreased with increasing gas flow velocity. Alternatively, it has been reported that the droplet diameter generated by the bag breakup in a cross-flow is generally independent of the Weber number (Ng, Sankarakrishnan & Sallam 2008). The bag breakup occurs when the liquid film is sufficiently thin, below the critical Weber number, regardless of how the gas flow is injected. Therefore, the fundamental characteristics of the bag breakup will be common. Measured droplet distributions at $x = 0$ mm and $z = 15$ mm are shown in figure 15. We can see a large variation in the droplet diameter since the film thickness and ligament diameter show large variations. We can confirm that the influence of the D_L and V_L on the diameter is very small, and the modal diameter lies between 8 and 12 μm. The predicted results agree well with the modal diameters.

Finally, predicted and measured droplet diameters were compared. Figure 16 shows the relationship between measured D_{10} obtained by PDI optical measurements and predicted D_{Bag}. As V_G increases from 40 to 80 m s^{-1}, measured values of D_{10} at $D_L = 0.2$ and 0.5 mm are almost constant. The order of predicted D_{Bag} agreed with measured D_{10}, indicating that the proposed model can capture the atomization phenomenon. However, there is a gap between D_{10} and predicted results, which indicates that we have to compare this with the other mean droplet diameter, e.g. modal diameter. The range of modal diameter is in the range of 6–20 μm for all conditions. However, it is difficult to determine at this stage which mean droplet diameter corresponds to the predicted droplet diameter. We will solve the problem in the near future.

We conclude, based on the above discussion, that the framework of the mechanistic model proposed in this study is plausible and provides an opportunity to predict the droplet diameter distribution produced by each elementary process of the atomization phenomenon.

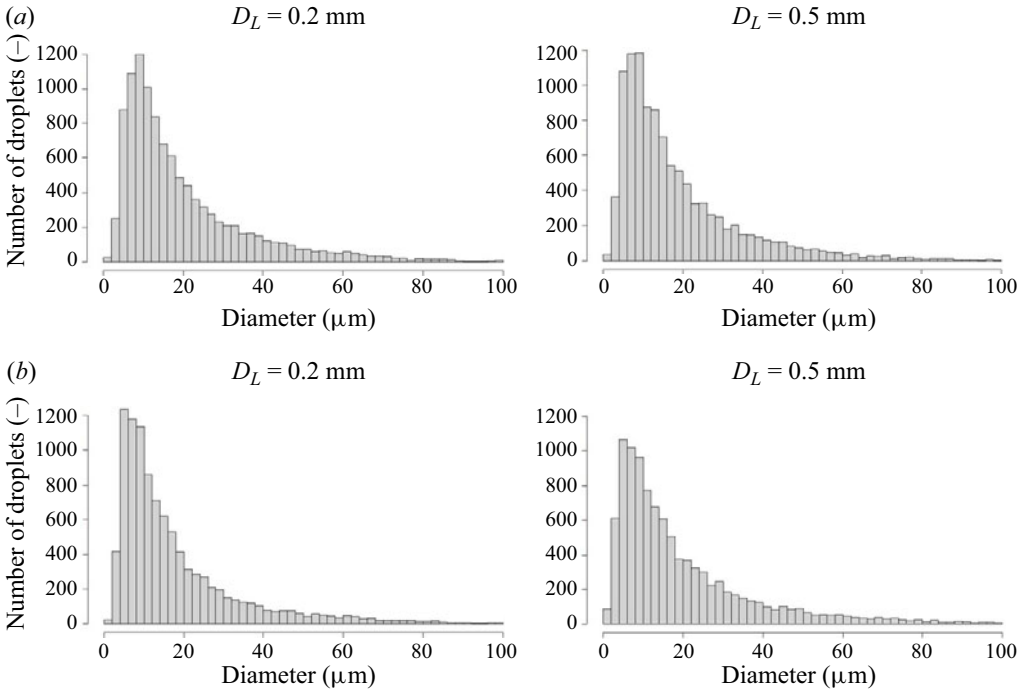

Figure 15. Droplet size distribution measured by PDI; (*a*) $V_L = 0.4$ m s^{-1}, $V_G = 80$ m s^{-1} and (*b*) $V_L = 0.4$ m s^{-1}, $V_G = 50$ m s^{-1}.

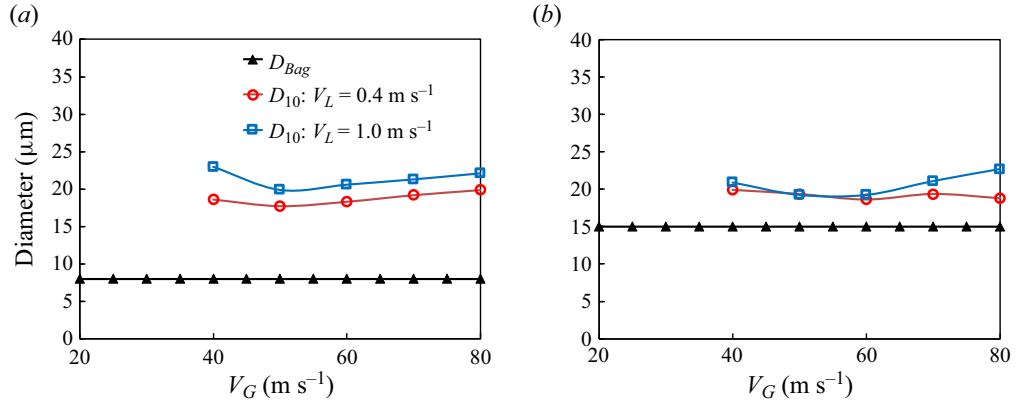

Figure 16. Predicted and measured droplet diameter by bag breakup; (*a*) $D_L = 0.2$ mm and (*b*) $D_L = 0.5$ mm.

5. Conclusions

The atomization process of the liquid film induced by the gas flow was investigated. The oscillation and breakup processes of the liquid film were initially discussed and modelled. Second, the bag breakup process was clarified using high-speed imaging. We validated our atomization model by measuring the droplet diameter using image analysis and PDI measurements. Consequently, we reached the following conclusions:

(i) We clarified for the first time that the film rupture is almost always caused by the impact of floating droplets on the expanding film of the bag, which is sufficiently thin.

(ii) The rim contraction velocity was in the range of 3–12 m s^{-1}. The effects of gas and liquid velocities on the contraction velocity were minimal in this study. The average film thickness immediately after bag rupture was 3–6 μm whose value is calculated by (2.12), and there was a considerable variation in film thickness, which may have contributed to the droplet size distribution.

(iii) The liquid at the perforation edge contracted, forming ligaments that fragmented the large droplets along the vertical and transverse rims.

(iv) We developed a mechanistic model for the droplet diameter distribution that provides the first framework for the air-blast atomization process. Its validity was verified by comparing the predicted and measured diameters using high-speed visualizations and optical measurements.

(v) The breakup of the ligament generates droplets of the order of submillimetres, while bag fragmentation generates tiny droplets with diameter in the micrometres range. The proposed model can roughly predict the droplet diameters.

Supplementary movie. A supplementary movie is available at https://doi.org/10.1017/jfm.2024.279.

Acknowledgements. The author would like to thank Mr K. Oishi for his help in the measurement and image analysis.

Funding. This study was supported by a JSPS KAKENHI Grant Numbers JP19K23489, 19KK0110 and JP21K14084.

Declaration of interests. The author reports no conflict of interest.

Author ORCIDs.
Ippei Oshima https://orcid.org/0000-0003-3739-0578;
Akira Sou https://orcid.org/0000-0003-0638-1767.

References

Agbaglah, G., Josserand, C. & Zaleski, S. 2013 Longitudinal instability of a liquid rim. *Phys. Fluids* **25** (2), 022103.

An, X., Dong, B., Zhang, Y., Geng, F., Zhou, X., Qin, Y. & Li, W. 2023 Effects of structured prefilmer lip on spray characteristics in planar prefilming airblast atomization. *Aerosp. Sci. Technol.* **140**, 108426.

Chou, W.-H. & Faeth, G.M. 1998 Temporal properties of secondary drop breakup in the bag breakup regime. *Intl J. Multiphase Flow* **24** (6), 889–912.

Culick, F.E.C. 1960 Comments on a ruptured soap film. *J. Appl. Phys.* **31** (6), 1128–1129.

Dombrowski, N. & Hooper, P.C. 1962 The effect of ambient density on drop formation in sprays. *Chem. Engng Sci.* **17** (4), 291–305.

Dombrowski, N. & Johns, W.R. 1963 The aerodynamic instability and disintegration of viscous liquid sheets. *Chem. Engng Sci.* **18** (3), 203–214.

Dumouchel, C. 2008 On the experimental investigation on primary atomization of liquid streams. *Exp. Fluids* **45** (3), 371–422.

Fernandez, V.G., Berthoumie, P. & Lavergne, G. 2009 Liquid sheet disintegration at high pressure: an experimental approach. *C. R. Méc.* **337** (6), 481–491.

Fraser, R.P., Eisenklam, P., Dombrowski, N. & Hasson, D. 1962 Drop formation from rapidly moving liquid sheets. *AIChE J.* **8** (5), 672–680.

Hagerty, W.W. & Shea, J.F. 1955 A study of the stability of plane fluid sheets. *J. Appl. Mech.* **22** (4), 509–514.

Inamura, T., Shirota, M., Tsushima, M., Kato, M., Hamajima, S. & Sato, A. 2012 Spray characteristics of prefilming type of airblast atomizer. In *12th Triennial International Conference on Liquid Atomization and Spray Systems, Heidelberg*.

Inoue, C., Yoshida, H., Kouwa, J., Iwaki, Y. & Itoh, M. 2021 Measurement and modeling of planar airblast spray flux distributions. *Intl J. Multiphase Flow* **137**, 103580.

JACKIW, I.M. & ASHGRIZ, N. 2022 Prediction of the droplet size distribution in aerodynamic droplet breakup. *J. Fluid Mech.* **940**.

KANT, P., PAIRETTI, C., SAADE, Y., POPINET, S., ZALESKI, S. & LOHSE, D. 2023 Bag-mediated film atomization in a cough machine. *Phys. Rev. Fluids* **8** (7), 74802.

KOOIJ, S., SIJS, R., DENN, M.M., VILLERMAUX, E. & BONN, D. 2018 What determines the drop size in sprays? *Phys. Rev.* X **8** (3), 031019.

LEFEBVRE, A.H. 1980 Airblast atomization. *Prog. Energy Combust. Sci.* **6** (3), 233–261.

LEFEBVRE, A.H. 1992 Energy considerations in twin-fluid atomization. *Trans. ASME: J. Engng Gas Turbines Power* **114** (1), 89–96.

LOHSE, D. & VILLERMAUX, E. 2020 Double threshold behavior for breakup of liquid sheets. *Proc. Natl Acad. Sci.* **117** (32), 18912–18914.

LOZANO, A., BARRERAS, F., SIEGLER, C. & LÖW, D. 2005 The effects of sheet thickness on the oscillation of an air-blasted liquid sheet. *Exp. Fluids* **39** (1), 127–139.

MATSUURA, K., SUZUKI, S., SUDA, M., IINO, J. & HAYASHI, S. 2008 Effects of swirl on spray characteristics of a counter-swirl airblast fuel injector. In *22nd European Conference on Liquid Atomization and Spray Systems*.

MCENTEE, W.R. & MYSELS, K.J. 1969 Bursting of soap films. I. An experimental study. *J. Phys. Chem.* **73** (9), 3018–3028.

NG, C.-L., SANKARAKRISHNAN, R. & SALLAM, K.A. 2008 Bag breakup of nonturbulent liquid jets in crossflow. *Intl J. Multiphase Flow* **34** (3), 241–259.

ODIER, N., BALARAC, G., CORRE, C. & MOUREAU, V. 2015 Numerical study of a flapping liquid sheet sheared by a high-speed stream. *Intl J. Multiphase Flow* **77**, 196–208.

OSHIMA, I. & SOU, A. 2019 Longitudinal oscillation of a liquid sheet by parallel air flows. *Intl J. Multiphase Flow* **110**, 179–188.

OSHIMA, I. & SOU, A. 2021 Transversal oscillation of a planar liquid sheet induced by co-current airflows. *Multiphase Sci. Technol.* **33** (2), 53–67.

OSHIMA, I., SOU, A., KAWABATA, R. & MATSUURA, K. 2017 Longitudinal wavelength of oscillating liquid sheet with air flow. In *55th AIAA Aerospace Sciences Meeting*.

RAYLEIGH, LORD 1878 On the instability of jets. *Proc. Lond. Math. Soc.* **1**, 4–13.

SQUIRE, H.B. 1953 Investigation of the instability of a moving liquid film. *Brit. J. Appl. Phys.* **4** (6), 167–169.

TANG, K., ADCOCK, T.A.A. & MOSTERT, W. 2023 Bag film breakup of droplets in uniform airflows. *J. Fluid Mech.* **970**, A9.

TAYLOR, G. 1959 The dynamics of thin sheets of fluid. III. Disintegration of fluid sheets. *Proc. R. Soc. Lond. Ser.* A. *Math. Phys. Sci.* **253** (1274), 313–321.

VARGA, C.M., LASHERAS, J.C. & HOPFINGER, E.J. 2003 Initial breakup of a small-diameter liquid jet by a high-speed gas stream. *J. Fluid Mech.* **497**, 405–434.

VILLERMAUX, E. 2006 Fragmentation. *Annu. Rev. Fluid Mech.* **39** (1), 419–446.

VILLERMAUX, E., MARMOTTANT, PH. & DUPLAT, J. 2004 Ligament-mediated spray formation. *Phys. Rev. Lett.* **92**, 074501.

WARNCKE, K., GEPPERTH, S., SAUER, B., SADIKI, A., JANICKA, J., KOCH, R. & BAUER, H.-J. 2017 Experimental and numerical investigation of the primary breakup of an airblasted liquid sheet. *Intl J. Multiphase Flow* **91**, 208–224.

WEBER, C. 1931 Zum Zerfall Eines Flüssigkeitsstrahles. *Z. Angew. Math. Mech.* **11** (2), 136–154.

YOSHIDA, K., IDE, K., TAKAHASHI, S., MATSUURA, K., IINO, J., KUROSAWA, Y., HAYASHI, S. & OHTA, Y. 2012 Airblast spray characteristics of planar liquid films in longitudinal gas-phase shear layers at various ambient pressure conditions. In *Proceedings of the 12th ICLASS*, 2012.

ZUZIO, D., ESTIVALEZES, J.-L., VILLEDIEU, P. & BLANCHARD, G. 2013 Numerical simulation of primary and secondary atomization. *C. R. Méc.* **341** (1), 15–25.